JOURNAL OF GUIDANCE, CONTROL, AND DYNAMICS
Vol. 28, No. 6, November–December 2005

Optimal Solar-Sail Trajectories for Missions to the Outer Solar System

Bernd Dachwald*
DLR, German Aerospace Center, 51147 Cologne, Germany

Although the solar radiation pressure decreases with the square of solar distance, solar sails enable missions to the outer solar system and even beyond. For such missions, the solar sail can gain a large amount of energy by first making one or more close approaches to the sun. Within this paper, optimal trajectories for solar-sail missions to the outer planets and into near interstellar space are presented, both for ideal and for nonideal sails. Therefore, also, near-/medium-term solar sails with a relatively moderate performance are considered. The minimum flight time to the outer solar system depends not only on the lightness of the solar sail, but also on the allowed minimum solar distance. The minimum solar distance, however, is constrained by the temperature limit of the sail film. Within this paper, it is demonstrated that faster trajectories can be obtained for a given sail temperature limit, if not, as usual, the allowed minimum solar distance, but the allowed maximum sail temperature is directly used as a path constraint for optimization. Although, especially for moderate-performance solar sails, the geometry of optimal trajectories becomes quite sophisticated, the required flight times and the achieved solar system escape velocities obey very simple laws.

Introduction

USING solely the freely available solar radiation pressure (SRP) for propulsion, solar sails enable a wide range of high-ΔV missions, many of which are difficult or even impossible to accomplish with any other type of conventional propulsion system. Solar sails enable even missions to the outer solar system and beyond, despite the fact that the SRP decreases with the square of the sun-sail distance. Sauer observed that the solar sail can gain a large amount of energy by making a close approach to the sun, turning the trajectory into a hyperbolic one,[1] a maneuver for which Leipold coined the term "solar photonic assist" (SPA).[2,3] Sauer made parametric studies for near-interstellar missions to 100 astronomical units (AU), 250 AU, and 1000 AU using ideal very high-performance solar sails that perform only a single SPA.[4] Leipold observed that solar sails with a more conservative performance require multiple SPAs to achieve solar-system escape. He calculated some trajectories for ideal solar sails, but made no parametric studies. Within this paper, optimal trajectories for solar-sail missions to the outer planets and into near interstellar space (200 AU, the maximum distance where the heliopause is expected to lie[5]) are presented, both for ideal and nonideal sails. It is shown that—even for near-/medium-term solar sails with relatively moderate performance—such SPA trajectories allow reasonable transfer times to the outer solar system without the need to perform any gravity-assist maneuver. Nevertheless, without the use of additional propulsive devices and/or an aerocapture maneuver at the target, only fast flybys can be accomplished because of the associated large hyperbolic excess velocities. The minimum flight time to an outer-solar-system target depends not only on the lightness of the solar sail, but also on the allowed minimum solar distance: the smaller the minimum solar distance, the larger the amount of energy that can be gained by a solar approach. The minimum solar distance, however, is limited by the temperature limit of the sail film. In the previous work by Sauer and Leipold, the allowed minimum solar distance was used as a path constraint for trajectory optimization, with the argument that such a constraint enforces that some sail temperature limit will not be exceeded during the closest solar approach. The sail temperature, however, depends not only on the solar distance, but also on the sail attitude. Within this paper, it is demonstrated that faster trajectories can be obtained for a given sail temperature limit, if not the allowed minimum solar distance, but the allowed maximum sail temperature is directly used as a path constraint for optimization. For the calculation of near-globally optimal trajectories, evolutionary neurocontrol is used, a method that is based on artificial neural networks and evolutionary algorithms.[6,7]

Presented as Paper 2004-5406 at the AIAA/AAS Astrodynamics Specialist Conference, Providence, RI, 16–20 August 2004; received 8 September 2004; revision received 12 November 2004; accepted for publication 15 November 2004.

*Research Engineer, Institute of Space Simulation, Linder Hoehe; bernd.dachwald@dlr.de. Member AIAA.

Solar-Sail Force Models

To describe the SRP force exerted on a solar sail, it is convenient to introduce two unit vectors. The first one is the sail normal vector $\boldsymbol{n}$, which is perpendicular to the sail surface and always directed away from the sun. Its direction, which describes the sail attitude, is expressed by the sail clock angle α and the sail cone angle β (Fig. 1a). The second unit vector is the thrust unit vector $\boldsymbol{f}$, which points always along the direction of the SRP force. Its direction is described likewise by the thrust clock angle γ and the thrust cone angle δ (Fig. 1b).

At a distance r from the sun, the SRP is

$$P = (S_0/c)(r_0/r)^2 = 4.563(\mu\mathrm{N/m^2}) \cdot (r_0/r)^2 \tag{1}$$

where $S_0 = 1368\ \mathrm{W/m^2}$ is the solar constant, c is the speed of light in vacuum, and $r_0 = 1$ AU. For the optical characteristics of a solar sail, different assumptions can be made, which result in different models for the magnitude and direction of the SRP force acting on the sail. The most simple model assumes an ideally reflecting sail surface. The SRP force on an ideal sail of area A is

$$\boldsymbol{F}_{\mathrm{SRP}} = 2PA\cos^2\beta\boldsymbol{n} \tag{2}$$

Thus, the SRP force is always along the direction of the sail normal vector, $\boldsymbol{f} = \boldsymbol{n}$.

Another SRP force model that is widely encountered uses an overall sail efficiency factor $\eta \leq 1$ with the intention of describing the nonideal reflectivity of the sail. Using this factor, the SRP force acting on the sail is

$$\boldsymbol{F}_{\mathrm{SRP}} = 2\eta PA\cos^2\beta\boldsymbol{n} \tag{3}$$

and hence again $\boldsymbol{f} = \boldsymbol{n}$. Therefore, this model describes also a specularly reflecting sail surface, where the angle of incidence is equal

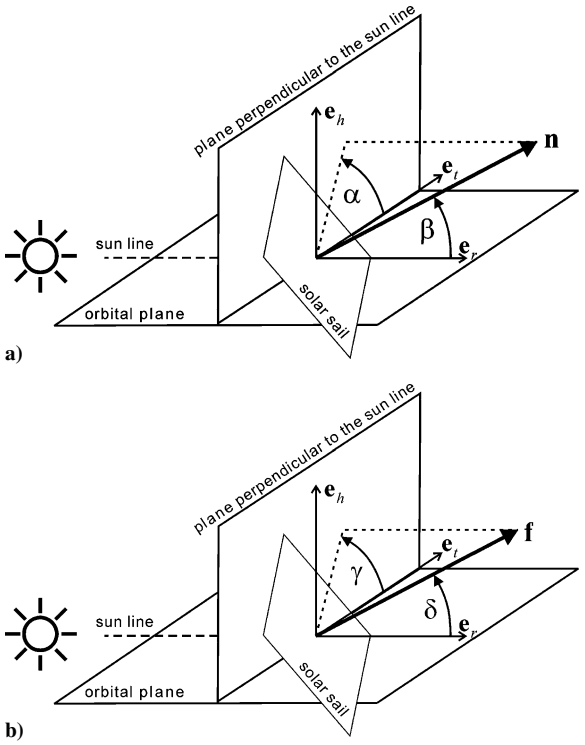

Fig. 1 Definition of a) the sail normal vector and b) the thrust unit vector.

to the angle of reflection. For trajectory analysis, this model does not need to be considered further because it is equivalent to the ideal sail model: a decrease of η can always be offset with an inversely proportional increase of A.

Because a real solar sail is not a specular reflector, a thorough trajectory simulation must consider the optical characteristics of the real sail film, as they can be parameterized by the absorption coefficient α, the reflection coefficient ρ, the transmission coefficient τ, and the emission coefficient ε, with the constraint $\alpha+\rho+\tau=1$. The reflection coefficient can be further divided into a coefficient for specular reflection ρ_s, a coefficient for diffuse reflection ρ_d, and a coefficient for backreflection ρ_b, with the constraint $\rho_s+\rho_d+\rho_b=\rho$. The nonideal solar-sail force model used in this paper considers the optical parameters $\mathcal{P}=\{\alpha, \rho_s, \rho_d, \rho_b, \tau, \varepsilon_f, \varepsilon_b\}$ of a sail film that is aluminum (A1) coated on the front side (high reflectivity) and chromium (Cr) coated on the back side (high emissivity) to keep the sail temperature within moderate limits, as will become clear later from Eq. (15). In this case, the SRP force has a component

$$F_\perp = 2PAq_\perp(\beta,\mathcal{P}) \tag{4}$$

perpendicular to the sail surface and a component

$$F_\parallel = 2PAq_\parallel(\beta,\mathcal{P}) \tag{5}$$

parallel to the sail surface. Using the optical parameters for an Al|Cr-coated sail ($\alpha=0.12$, $\rho_s=0.8272$, $\rho_d=0.0528$, $\rho_b=0$, $\tau=0$, $\varepsilon_f=0.05$, $\varepsilon_b=0.55$) (Ref. 8), and neglecting the degradation of the optical characteristics of the sail film over time caused by the erosive effects of the space environment, one gets

$$q_\perp(\beta,\mathcal{P}_{\text{Al|Cr}}) = 0.9136\cos^2\beta - 0.005444\cos\beta \tag{6}$$

$$q_\parallel(\beta,\mathcal{P}_{\text{Al|Cr}}) = 0.0864\sin\beta\cos\beta \tag{7}$$

The SRP force can be written as

$$\boldsymbol{F}_{\text{SRP}} = \sqrt{F_\perp^2+F_\parallel^2}\,\boldsymbol{f} \tag{8}$$

and by defining

$$Q^2(\beta,\mathcal{P}) = \sqrt{q_\perp^2(\beta,\mathcal{P})+q_\parallel^2(\beta,\mathcal{P})} \tag{9}$$

as

$$\boldsymbol{F}_{\text{SRP}} = 2PAQ^2(\beta,\mathcal{P})\boldsymbol{f} \tag{10}$$

Thus, the SRP force is not along the direction of the sail normal vector (except for $\beta=0$). The angle between $\boldsymbol{n}$ and $\boldsymbol{f}$ is arctan $(q_\parallel/q_\perp)$.

The following performance parameters are commonly used to describe the lightness of solar sailcraft: The sail assembly loading is defined as the mass of the sail assembly [the sail film and the required structure for storing, deploying, and tensioning the sail, index (SA)] per unit area:

$$\sigma_{\text{SA}} = m_{\text{SA}}/A \tag{11}$$

The sail-assembly loading is the key parameter for the efficiency of the solar sail's structural design. The sailcraft loading is the key parameter for the lightness of the entire solar sailcraft. It is defined as the specific mass of the sailcraft including the payload (index PL), where the term payload stands for the total sailcraft except the solar-sail assembly, that is, except the propulsion system:

$$\sigma = m/A = (m_{\text{SA}}+m_{\text{PL}})/A = \sigma_{\text{SA}} + m_{\text{PL}}/A \tag{12}$$

The characteristic acceleration is an equivalent parameter for expressing the lightness of the entire solar sailcraft. It is defined as the SRP acceleration acting on a solar sailcraft with the solar sail oriented perpendicular to the sun line at 1 AU distance from the sun:

$$a_c = 2S_0/c\cdot q_\perp(0,\mathcal{P})\cdot A/m = P_{\text{eff},0}(\mathcal{P})\cdot A/m$$
$$= P_{\text{eff},0}(\mathcal{P})/(\sigma_{\text{SA}}+m_{\text{PL}}/A) \tag{13}$$

For an Al|Cr-coated sail, the effective SRP at 1 AU is $P_{\text{eff},0}(\mathcal{P}_{\text{Al|Cr}}) = 2S_0/c\cdot q_\perp(0,\mathcal{P}_{\text{Al|Cr}}) = 8.288\,\mu\text{N/m}^2$. The lightness number is another equivalent parameter for expressing the lightness of the entire solar sailcraft. It is defined as the ratio of the SRP acceleration acting on a solar sailcraft with the solar sail oriented perpendicular to the sun line and the gravitational acceleration of the sun ($a_0=5.93\,\text{mm/s}^2$ at 1 AU). The lightness number of solar sailcraft can be defined as

$$\lambda = a_c/a_0 \tag{14}$$

because both the SRP and the gravitational acceleration vary with $1/r^2$.

Solar-Sail Orbital Dynamics

The thrust vector of a solar sail is constrained to lie on the surface of a bubble that is always directed away from the sun (Fig. 2). Nevertheless, by controlling the sail orientation relative to the sun, a solar sail can gain orbital angular momentum (if $\boldsymbol{F}_{\text{SRP}}\cdot\boldsymbol{e}_t>0$) and spiral outward, away from the sun, or lose orbital angular momentum (if $\boldsymbol{F}_{\text{SRP}}\cdot\boldsymbol{e}_t<0$) and spiral inward, toward the sun. For SPA trajectories, the minimum flight time depends not only on the lightness of the solar sail, but also on the minimum solar distance along the trajectory.

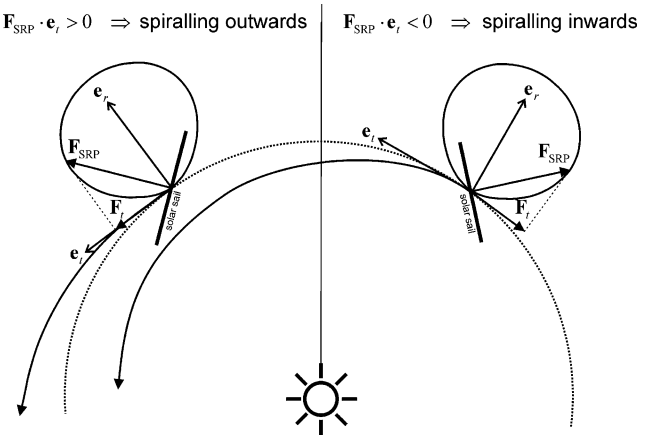

Fig. 2 Spiralling toward and away from the sun.

The smaller the solar distance is, the larger the amount of energy that can be gained by a SPA. The sail's equilibrium temperature at a distance r from the sun is[9]

$$T = \left[(1-\rho)/(\varepsilon_f + \varepsilon_b)(S_0/\sigma)\left(r_0^2/r^2\right)\cos\beta\right]^{\frac{1}{4}} \propto \left(\cos^{\frac{1}{4}}\beta/r^{\frac{1}{2}}\right) \tag{15}$$

where $\sigma = 5.67051 \cdot 10^{-8}\mathrm{Wm}^{-2}\mathrm{K}^{-4}$ is the Stefan–Boltzmann constant. Therefore, the minimum distance to the sun is, for a given sail attitude, limited by the temperature limit of the sail film. Trajectory optimization for SPA trajectories is exceedingly difficult because one must not only beware of flying too close to the sun, but one must also take care that the trajectory does not become hyperbolic too early, so that no additional energy can be gained. At the same time, one must find the optimal tradeoff between the time that is spent within the inner solar system to gain energy and the time that is required to fly outwards after the trajectory became hyperbolic. Simple guidance strategies typically yield nonoptimal trajectories, where the solar sail wastes time in a large elliptical orbit before the final SPA.[10]

Evolutionary Neurocontrol: Smart Global Low-Thrust Trajectory Optimization Method

In this paper, evolutionary neurocontrol (ENC) is used for the calculation of near-globally optimal trajectories. This method is based on artificial neural networks (ANN) and evolutionary algorithms (EA). ENC attacks low-thrust trajectory optimization problems from the perspective of artificial intelligence and machine learning. Here, it can only be sketched how this method is used to search optimal solar-sail trajectories. The reader who is interested in the details of the method is referred to Refs. 6 and 7. The problem of searching an optimal solar-sail trajectory $\boldsymbol{x}^\star[t] = (r^\star[t], \dot{r}^\star[t])$ (where the symbol $[t]$ denotes the time history of the preceding variable and the symbol $\star$ denotes its optimal value) is equivalent to the problem of searching an optimal sail normal vector history $\boldsymbol{n}^\star[t]$, as it is defined by the optimal time history of the so-called direction unit vector $\boldsymbol{d}^\star[t]$, a unit vector that points along the optimal thrust direction. Within the context of machine learning, a trajectory is regarded as the result of a sail steering strategy S that maps the problem relevant variables (the solar-sail state $\boldsymbol{x}$ and the target state $\boldsymbol{x}_T$) onto the direction unit vector $\mathsf{S} : \{\boldsymbol{x}, \boldsymbol{x}_T\} \subset \mathbb{R}^{12} \mapsto \{\boldsymbol{d}\} \subset \mathbb{R}^3$, from which $\boldsymbol{n}$ is calculated. This way, the problem of searching $\boldsymbol{x}^\star[t]$ is equivalent to the problem of searching (or learning) the optimal sail steering strategy $\mathsf{S}^\star$. An ANN can be used as a so-called neurocontroller (NC) to implement solar-sail steering strategies. It can be regarded as a parameterized function N_π (the network function), that is, for a fixed network geometry, completely defined by the internal parameter set π of the ANN. Therefore, each π defines a sail steering strategy S_π. The problem of searching $\boldsymbol{x}^\star[t]$ is therefore equivalent to the problem of searching the optimal NC parameter set $\pi^\star$. EAs that work on a population of strings can be used for finding $\pi^\star$ because π can be mapped onto a string ξ (also called chromosome or individual). The trajectory optimization problem is solved when the optimal chromosome $\xi^\star$ is found. Figure 3 sketches the subsequent transformation of a chromosome into a solar-sail trajectory. An evolutionary neurocontroller (ENC) is a NC that employs an EA for learning (or breeding) $\pi^\star$. ENC was implemented by the author within a low-thrust trajectory optimization program called InTrance, which stands for intelligent trajectory optimization using neurocontroller evolution. InTrance is a smart global trajectory optimization method that requires only the target body/state and intervals for the initial conditions (e.g., launch date, hyperbolic excess velocity, etc.) as input to find a near-globally optimal trajectory for the specified problem. It works without an initial guess and does not require the attendance of a trajectory optimization expert.

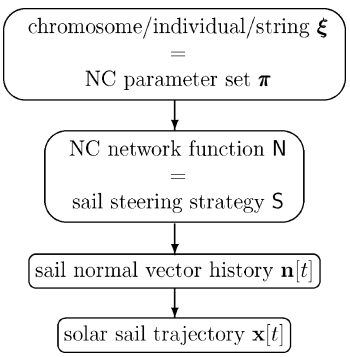

Fig. 3 Transformation of a chromosome into a solar-sail trajectory.

Results

All trajectories calculated within this paper assume direct interplanetary insertion of the solar sail with zero hyperbolic excess energy ($C_3 = 0$ km^2/s^2). To find the absolute flight time minima, independent of the actual constellation of Earth and the respective target, no flyby at the target itself, but only a crossing of its orbit within a distance of less than 10^6 km was required, and InTrance was allowed to vary the launch date within a one-year interval. Therefore, the resulting flight times represent lower bounds that are strictly valid only for the optimal constellation of Earth and the respective target. Specific suboptimal launch dates/constellations, for example, when the target is at aphelion, might yield much longer flight times. Although a final distance of 10^6 km is relatively large for a planetary flyby, the control profile found by InTrance can be used as an initial guess for some local trajectory optimization method with a better local convergence behavior. Alternatively, the neurocontroller parameters found by InTrance can be used as an initial guess for another run of InTrance (with a more demanding final constraint, e.g., 1000 km above the planetary surface).

Besides the gravitational forces of all celestial bodies and the SRP force, many disturbing forces, as caused, for example, by the solar wind and the aberration of solar radiation (Poynting–Robertson effect), influence the motion of solar sails. Ideally, all of these forces have to be considered for a thorough mission analysis. For mission feasibility analysis, however, as it is done within this paper, the following simplifications are valid: 1) the solar sail is moving under the sole influence of solar gravitation and radiation, 2) the sun is a point mass and a point light source, 3) the solar-sail attitude can be changed instantaneously, and 4) the optical characteristics of the sail film do not degrade over time.

Later in this paper it will become necessary to distinguish trajectories, for which the allowed minimum solar distance was limited, from trajectories, for which the allowed maximum sail film temperature was limited. Therefore, let r_{lim} denote the allowed minimum solar distance (distance limit) and r_{min} the minimum solar distance along the trajectory, and let T_{lim} denote the allowed maximum sail film temperature (sail temperature limit) and T_{max} the maximum sail film temperature along the trajectory. Using this notation, $T_{\mathrm{max}} = T_{\mathrm{max}}(r_{\mathrm{lim}})$ for distance-limited trajectories, and $r_{\mathrm{min}} = r_{\mathrm{min}}(T_{\mathrm{lim}})$ for temperature-limited trajectories.

Before calculating minimum flight times $\mathcal{T}$ and solar-system escape velocities v_{esc} for missions to all outer planets and into near interstellar space (200 AU), a Neptune flyby mission will be used to assess the general features of SPA trajectories, to compare different solar sail force models (ideal vs nonideal solar sails) and to compare different optimization constraints (limitation of allowed minimum solar distance vs limitation of allowed maximum sail temperature). [$v_{\mathrm{esc}} = \sqrt{(v_f^2 - 2\mu/r_f)}$, where v_f is the final velocity, r_f is the final solar distance, and μ is the sun's gravitational constant.] Finally, by calculating optimal temperature-limited trajectories for nonideal solar sails, it will be investigated how the minimum flight time, the solar-system escape velocity, and the geometry of the trajectory (e.g., the number of SPAs) vary for a wide range of characteristic accelerations and different sail temperature limits.

Minimum Flight Times for Ideal Solar Sails

For a Neptune flyby, InTrance was used to calculate minimum flight times for ideal solar sails with different characteristic accelerations (0.5 mm/s^2 $\le a_c \le$ 2.0 mm/s^2) and different solar distance limits (0.1 AU $\le r_{\mathrm{lim}} \le$ 0.5 AU). Figure 4 shows that the trajectories are faster for lighter solar sails and for sails that are allowed

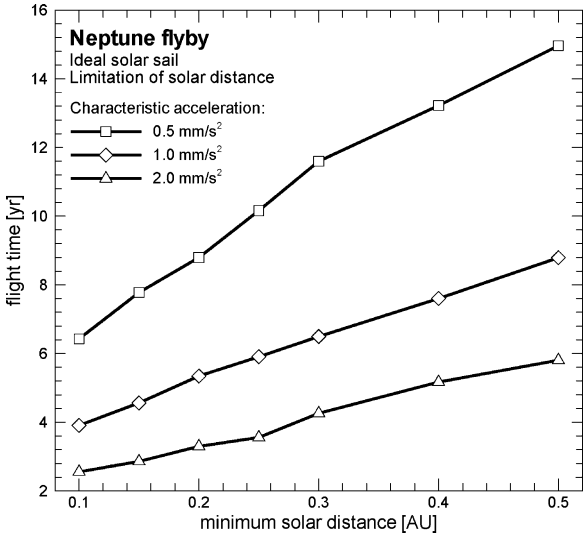

Fig. 4 Minimum flight time over minimum solar distance for different characteristic accelerations.

to approach the sun closely. Independent of r_{lim}, the optimal trajectories make a single SPA for $a_c = 2.0$ mm/s^2, a double SPA for $a_c = 1.0$ mm/s^2, and a triple SPA for $a_c = 0.5$ mm/s^2. The minimum flight times obey approximately a linear law for all three values of a_c:

$$\mathcal{T}(a_c, r_{\text{lim}}) \approx c_1(a_c) r_{\text{lim}} + c_2(a_c)$$

Figure 5 shows optimal Neptune flyby trajectories for four different characteristic accelerations, the allowed minimum solar distance being limited to $r_{\text{lim}} = 0.1$ AU (which is very low for conventional sail films) in all four cases. One can see that more and more SPAs are required as the characteristic acceleration of the sail decreases. The optimal trajectory for the lightest solar sail ($a_c = 2.0$ mm/s^2) makes only a single SPA, whereas the optimal trajectory for the heaviest solar sail ($a_c = 0.5$ mm/s^2) requires four SPAs to reach Neptune in minimum time. The lower the characteristic acceleration of the solar sail, the larger also the fraction of flight time that must be spent in the inner solar system for gaining orbital energy (30.1% of total flight time for $a_c = 2.0$ mm/s^2, 33.5% for $a_c = 1.0$ mm/s^2, 39.9% for $a_c = 0.75$ mm/s^2, and 44.5% for $a_c = 0.5$ mm/s^2). For solar sailcraft with a low characteristic acceleration, the larger flight time fraction in the inner solar system can—additionally to the longer total flight time—render sail film degradation a serious problem.

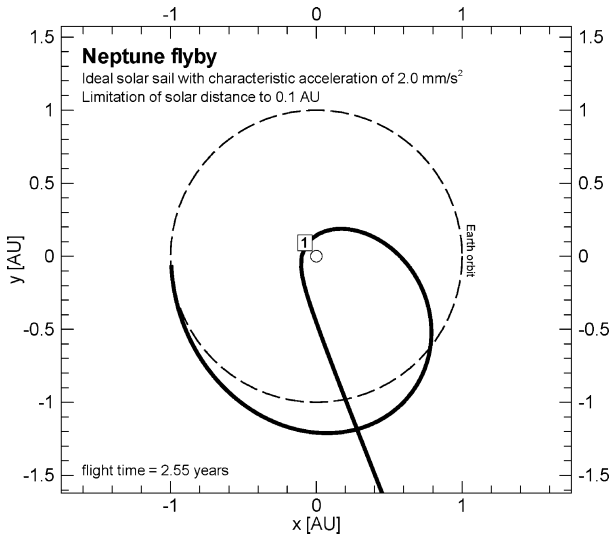

a) $a_c = 2.0$ mm/s^2, one solar photonic assist

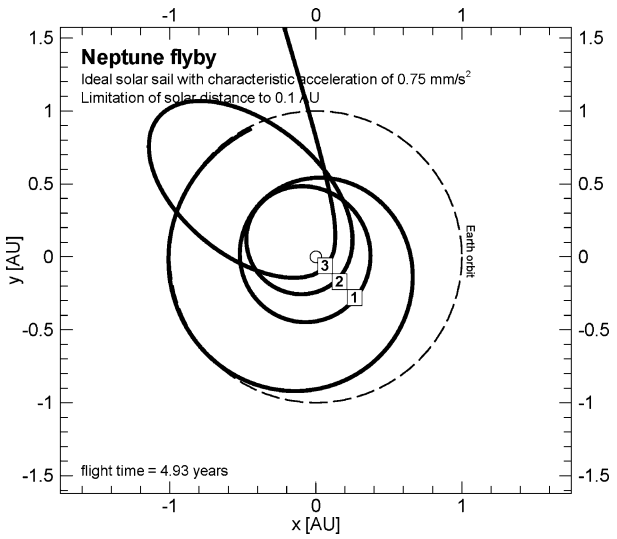

c) $a_c = 0.75$ mm/s^2, three solar photonic assists

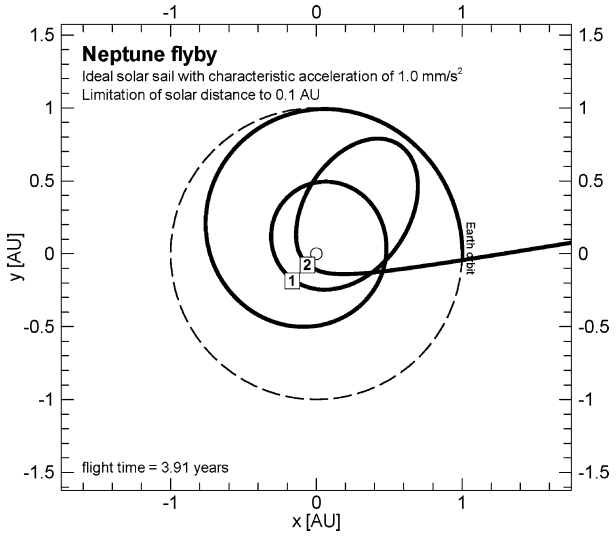

b) $a_c = 1.0$ mm/s^2, two solar photonic assists

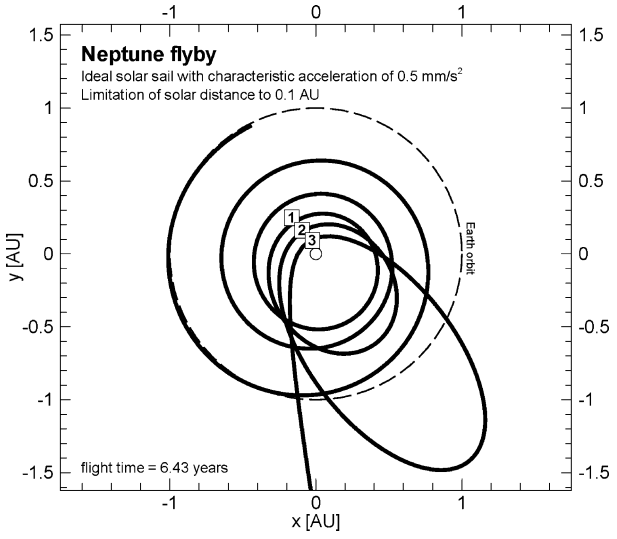

d) $a_c = 0.5$ mm/s^2, three solar photonic assists

Fig. 5 Geometry of optimal Neptune flyby trajectories for different characteristic accelerations.

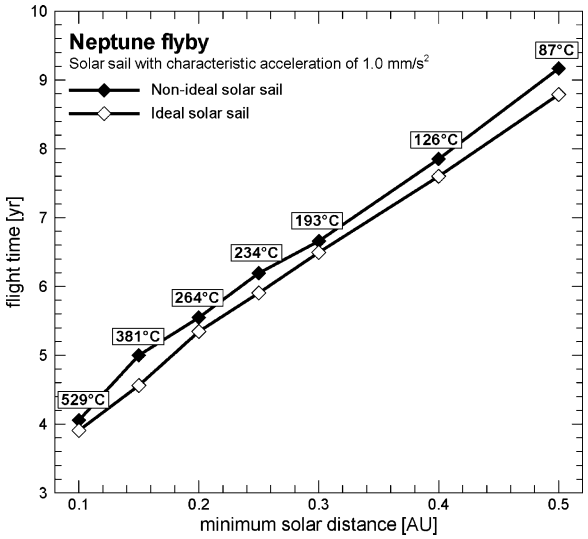

Fig. 6 Comparison of minimum flight times for ideal and nonideal solar sails.

Ideal vs Nonideal Solar Sails

In the preceding section, minimum flight times have been presented for ideal solar sails because, to the author's knowledge, all previous solar-sail trajectory analyses for solar-system escape missions assume ideal reflectivity of the sail. A real solar sail, however, is not an ideal reflector, and a thorough trajectory analysis must take into account the optical characteristics of the real sail film.[11] In Fig. 6, flight times are compared for an ideal and a nonideal solar sail, both with $a_c = 1.0$ mm/s^2. Figure 6 shows that the flight times are about 5% longer, if the nonideal reflectivity of the sail is taken into account.

Distance-Limited vs Temperature-Limited Trajectories

In the previous work by Sauer,[4] Leipold and Wagner,[2] and Leipold,[3] r_{lim} was used as a path constraint for the trajectory optimization of ideal solar sails, with the argument that such a constraint enforces that some T_{lim} will not be exceeded during the closest solar approach [although strictly, according to Eq. (15), the temperature of an ideal sail is always 0 K because $\rho = 1$]. According to Eq. (15), however, the temperature at a given solar distance r depends also on the light incidence angle β. It might therefore yield faster trajectories for a given T_{lim}, if not r_{lim}, but T_{lim} is directly used as a path constraint. This can be realized by constraining the sail attitude so that the light incidence angle can not become smaller than the critical one, $\beta > \beta_{\text{lim}}(r, T_{\text{lim}})$, where T_{lim} would be exceeded. Figure 7 shows two exemplary trajectories, one distance limited (Fig. 7a) and one temperature limited (Fig. 7b). By keeping β large enough during the closest solar approach, the temperature-limited trajectory approaches the sun closer while maintaining the sail temperature below the temperature that is given by the distance-limited trajectory (so that $T_{\max}$ is the same for both trajectories). The resulting trajectory is faster than the distance-limited one. Figure 8 shows that for a given T_{lim}, optimal temperature-limited trajectories are on average about 5% faster than optimal distance-limited ones. The minimum flight times and the maximum sail temperatures are nearly inversely proportional for both curves:

$$\mathcal{T}(T_{\max}) \approx c_3 / T_{\max}$$

Minimum Flight Times to the Outer Planets and into Near Interstellar Space

Figure 9 shows the minimum flight times $\mathcal{T}$ and the achieved solar-system escape velocities v_{esc} for optimal temperature-limited flyby trajectories to the outer planets and to 200 AU using a nonideal solar sail. The sail film temperature was limited to $T_{\text{lim}} = 240°$C. The minimum flight times obey approximately a potential law for all targets,

$$\mathcal{T}(\text{Target}, a_c) \approx c_4(\text{Target}) a_c^{c_5(\text{Target})}$$

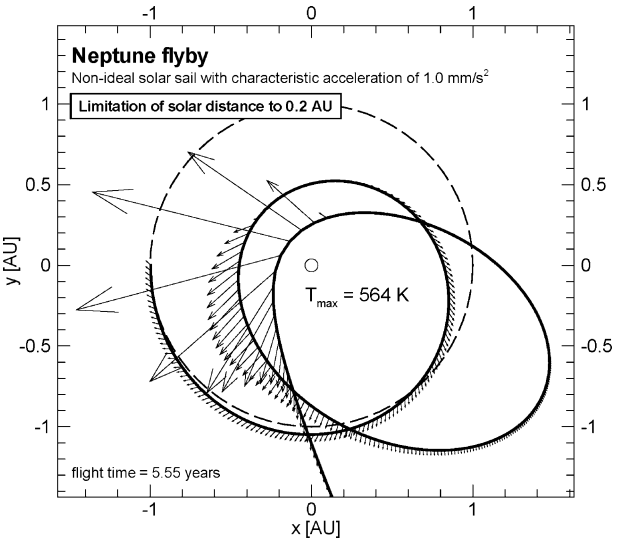

a) Distance-limited trajectory

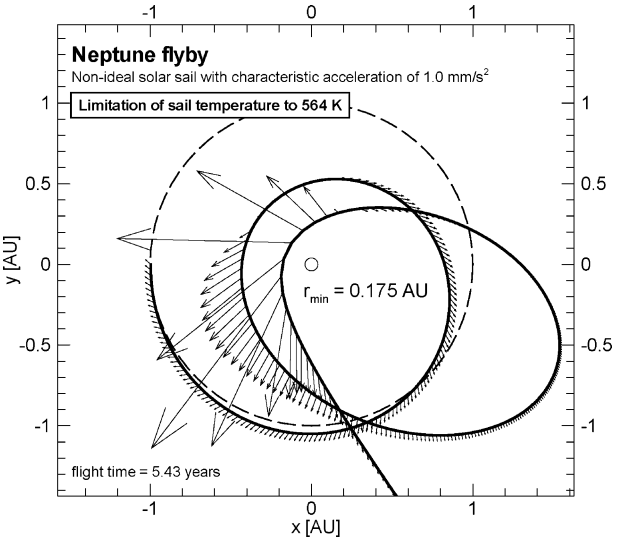

b) Temperature-limited trajectory

Fig. 7 Optimal Neptune flyby trajectories for different optimization constraints.

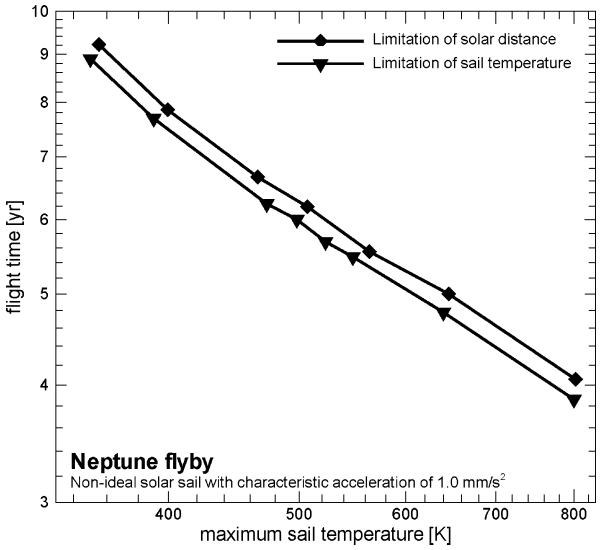

Fig. 8 Minimum flight time over maximum sail temperature for distance-limited and temperature-limited trajectories.

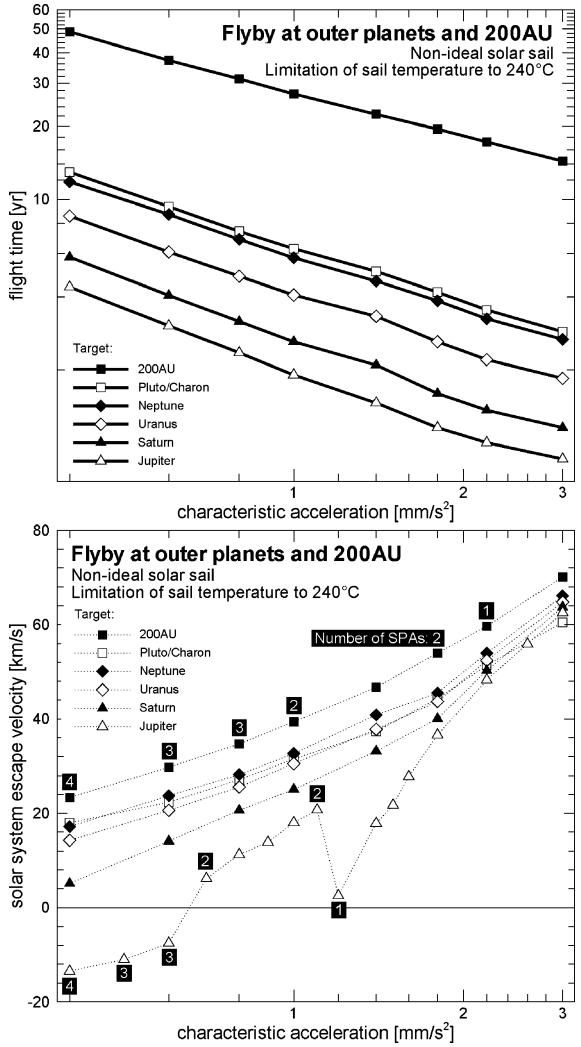

Fig. 9 Optimal temperature-limited flyby at outer planets.

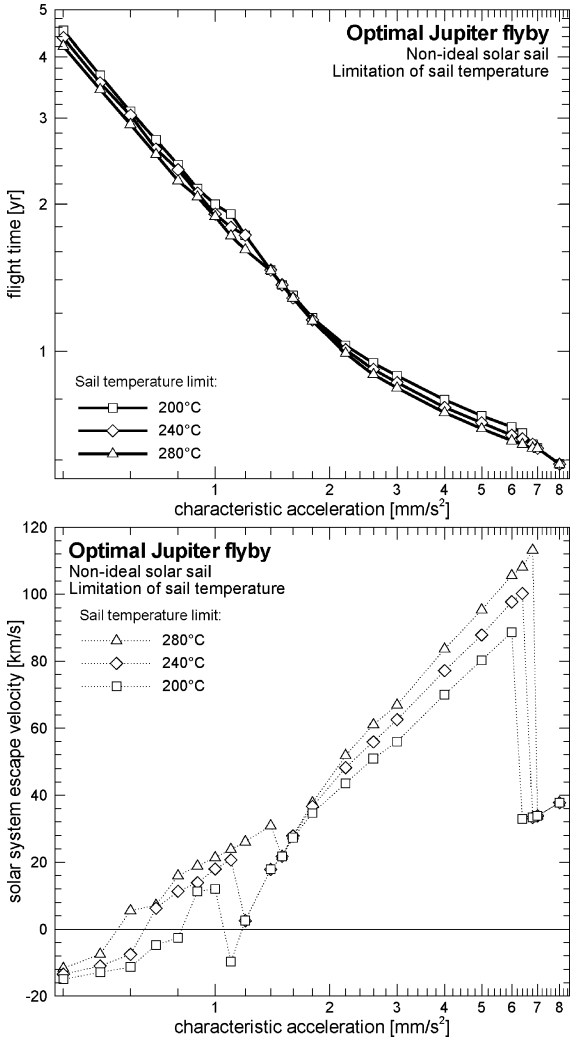

Fig. 10 Optimal temperature-limited Jupiter flyby.

with $-0.827 < c_5(\text{Target}) < -0.601$. Figure 9 shows that v_{esc} increases for more distant targets because it is beneficial, in this case, to spend more time in the inner solar system to gain more energy. Figure 9 shows that even near-term solar sails ($a_c \approx 0.4$ mm/s^2) are able to reach Uranus within less than 10 years and that even medium-term solar sails ($a_c \approx 0.6$ mm/s^2) are able to reach Neptune and the inner Edgeworth–Kuiper belt within less than 10 years. A more advanced solar sail, $a_c = 1.4$ mm/s^2, can reach 200 AU within less than 25 years. The v_{esc} curve for Jupiter shows that for some values of a_c the optimal trajectories do not maximize v_{esc}. For $a_c = 1.2$ mm/s^2, for example, only a single SPA is performed. A double SPA would yield a larger v_{esc}, but would also require additional time for the second close solar approach. This is not time optimal because Jupiter is relatively close to the sun. The v_{esc} curves for more distant targets indicate no such discontinuity because the high-v_{esc} trajectories are also the fastest ones. The time-optimal Jupiter flyby trajectory for $a_c \lessapprox 0.65$ mm/s^2 is not a hyperbolic, but an elliptic one ($v_{\text{esc}} < 0$ km/s). Because of the interesting features of Jupiter's v_{esc} curve, optimal trajectories have been calculated for a wider range of characteristic accelerations (0.4 mm/s$^2 \le a_c \le 8.0$ mm/s^2) and for three different sail temperature limits (200, 240, and 280°C). The results for those calculations, shown in Fig. 10, will be described in the next section. A translation of the sail temperature limits into sail film materials is not within the scope of this paper because the allowed maximum sail film temperature depends not only on the film material, but also on the sail design (stresses, wrinkles, etc.).

Minimum Flight Times for Different Sail Temperature Limits

Figure 10 shows for three different sail temperature limits (200, 240, and 280°C) the minimum flight times and the achieved solar-system escape velocities for temperature-limited optimal flyby trajectories to Jupiter. One can see that there is for all three temperature limits a discontinuity in the v_{esc} curve, like the one observed in Fig. 9, but at different characteristic accelerations. For a lower T_{lim}, the optimal trajectory employs a single SPA down to lower characteristic accelerations, until a double SPA is optimal. If one considers also very large characteristic accelerations, a second discontinuity occurs in the range 6 mm/s$^2 \lessapprox a_c \lessapprox 7$ mm/s^2 because of a change in the geometry of the optimal trajectory: the optimal trajectories for $a_c \gtrapprox 7$ mm/s^2 do not make a SPA because this would take longer than a direct trajectory to Jupiter. Direct trajectories are feasible in this performance regime because for $\lambda = a_c/a_0 > 1$ the sail's acceleration capability is more than enough to cancel the solar gravitation, so that the solar sail is able to fly directly away from the sun. Figure 10 shows also that the flight time does not depend considerably on T_{lim} or v_{esc}, but only on a_c. Within the low-/medium-performance regime ($a_c \lessapprox 2.0$ mm/s^2) and the very high-performance regime ($a_c \gtrapprox 3.0$ mm/s^2), the minimum flight times obey nearly a potential law:

$$\mathcal{T}(a_c) \approx c_4 a_c^{c_5}$$

(c_4 and c_5 being different for both regimes), with a transition regime, where the $\mathcal{T}(a_c)$ curve bends.

Figure 11 shows for three different sail temperature limits (200, 240, and 280°C) the minimum flight times and the achieved solar-system escape velocities for temperature-limited optimal transfers to 200 AU. The minimum flight times and the achieved solar-system escape velocities obey a potential law for all sail temperature limits,

$$\mathcal{T}(a_c, T_{\text{lim}}) = c_4(T_{\text{lim}}) a_c^{c_5}$$

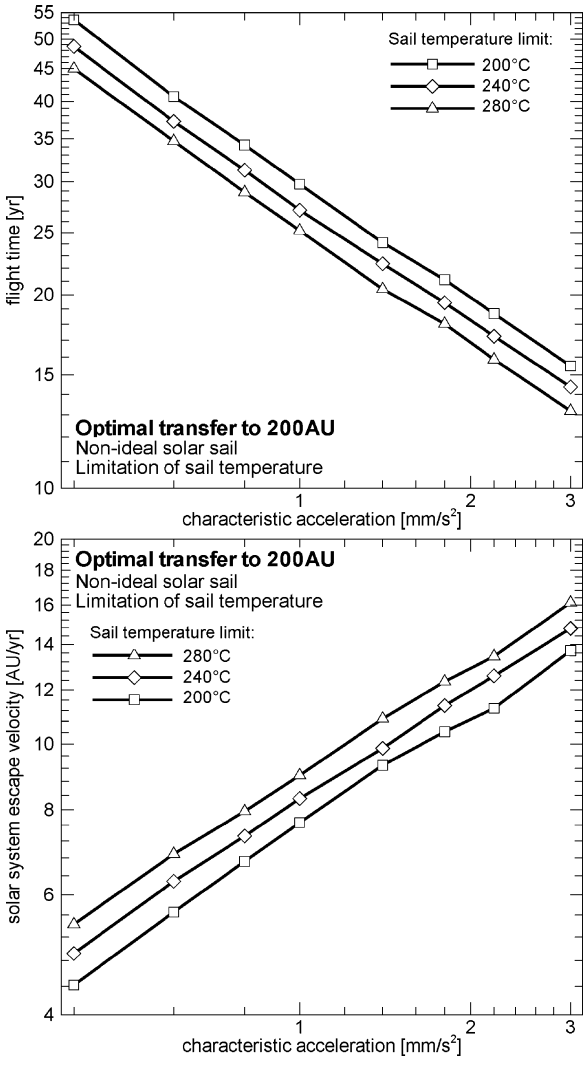

Fig. 11 Optimal temperature-limited transfer to 200 AU.

with $c_5 = 0.543^{\pm 0.011}$ and

$$v_{\mathrm{esc}}(a_c, T_{\mathrm{lim}}) = c_6(T_{\mathrm{lim}})a_c^{c_7}$$

with $c_7 = -0.605^{\pm 0.006}$. Both c_5 and c_7 do not depend on T_{lim}. Figure 11 shows that the minimum flight times to 200 AU depend considerably on the sail temperature limit ($r_{\min}$ varies also considerably with T_{lim}, but little with a_c: 0.222 AU $< r_{\min} <$ 0.238 AU for $T_{\mathrm{lim}} = 200°$C, 0.195 AU $< r_{\min} <$ 0.204 AU for $T_{\mathrm{lim}} = 240°$C, 0.165 AU $< r_{\min} <$ 0.181 AU for $T_{\mathrm{lim}} = 280°$C). For $T_{\mathrm{lim}} = 280°$C, a characteristic acceleration of about 1.0 mm/s^2 is required to reach 200 AU within 25 years from launch, whereas a characteristic acceleration of about 1.4 mm/s^2 is required for $T_{\mathrm{lim}} = 200°$C. Note that the solar-sail design parameters are typically very sensitive with respect to the characteristic acceleration, as the following example can show: if a solar sail with a sail assembly loading of $\sigma_{\mathrm{SA}} = 5$ g/m^2 should be used to transport a payload (including spacecraft bus) of $m_{\mathrm{PL}} = 100$ kg to 200 AU, $a_c = 1.0$ mm/s^2 yields according to Eq. (13) a sail area of $A = (175\,\mathrm{m})^2$, whereas $a_c = 1.4$ mm/s^2 yields a sail area of $A = (330\,\mathrm{m})^2$. If the sail size is held fixed at $(175\,\mathrm{m})^2$, the payload reduces to $m_{\mathrm{PL}} = 28$ kg. Another possibility is to decrease the sail assembly loading to $\sigma_{\mathrm{SA}} = 2.6$ g/m^2, which can only be done with some much more advanced sail fabrication/deployment technology.

Conclusions

The material presented within this paper provides, for a wide range of solar-sail performance levels and sail temperature limits, trajectory and performance tradeoffs for missions to the outer solar system and into near interstellar space. It was shown that a thorough trajectory analysis must consider the nonideal reflectivity of the solar sail, which yields minimum flight times that are about 5% longer than those of ideal sails. It was also shown that faster trajectories can be obtained for a given sail temperature limit, if not, as usual, the allowed minimum solar distance, but the allowed maximum sail temperature is directly used as a path constraint for optimization. Although, especially for moderate-performance solar sails, the geometry of optimal trajectories becomes quite sophisticated, the required flight times and the achieved solar system escape velocities obey very simple laws that are, however, not yet theoretically understood.

References

[1]Sauer, C. G., "Optimum Solar-Sail Interplanetary Trajectories," AIAA Paper 76-792, Aug. 1976.

[2]Leipold, M., and Wagner, O., "'Solar Photonic Assist' Trajectory Design fo Solar Sail Missions to the Outer Solar System and Beyond," *Spaceflight Dynamics 1998*, edited by T. H. Stengle, *Advances in the Astronautical Sciences*, Vol. 100, Pt. 2, 1998, pp. 1035–1045.

[3]Leipold, M., "To the Sun and Pluto with Solar Sails and Micro-Sciencecraft," *Acta Astronautica*, Vol. 45, Nos. 4–9, 1999, pp. 549–555.

[4]Sauer, C. G., "Solar Sail Trajectories for Solar Polar and Interstellar Probe Missions," *Astrodynamics 1999*, edited by K. Howell, F. Hoots, and B. Kaufman, *Advances in the Astronautical Sciences*, Vol. 103, 2000, pp. 547–562.

[5]de Pater, I., and Lissauer, J. J., *Planetary Sciences*, Cambridge Univ. Press, Cambridge, England, U.K., 2001, p. 5.

[6]Dachwald, B., "Optimization of Interplanetary Solar Sailcraft Trajectories Using Evolutionary Neurocontrol," *Journal of Guidance, Control, and Dynamics*, Vol. 27, No. 1, 2004, pp. 66–72.

[7]Dachwald, B., "Evolutionary Neurocontrol: A Smart Method for Global Optimization of Low-Thrust Trajectories," AIAA Paper 2004-5405, Aug. 2004.

[8]Wright, J. L., *Space Sailing*, Gordon and Breach, Philadelphia, 1992, p. 228.

[9]McInnes, C. R., *Solar Sailing. Technology Dynamics and Mission Applications*, Springer-Verlag, London, 1999, p. 49.

[10]Sharma, D. N., and Scheeres, D. J., "Solar-System Escape Trajectories Using Solar Sails," *Journal of Spacecraft and Rockets*, Vol. 41, No. 4, 2004, pp. 684–687.

[11]Dachwald, B., "Minimum Transfer Times for Nonperfectly Reflecting Solar Sailcraft," *Journal of Spacecraft and Rockets*, Vol. 41, No. 4, 2004, pp. 693–695.